

Design of a Triple Band Notched Compact FSS at UWB Frequency Range

Kanishka Katoch, Naveen Jaglan*, and Samir D. Gupta

Abstract—This article presents a bandstop Frequency Selective Surface (FSS) prototype based on square split ring resonators (SSRRs) and a square loop (SL) structure for Ultra Wide Band (UWB) frequency range. Triple band notches are obtained at WiMAX (3.3–3.6 GHz), WLAN (5–6 GHz), and Satellite communication X-band (7.2–8.4 GHz). To make this proposed design work as a band-stop filter, two SSRRs are positioned at the top layer of the substrate to resonate at WiMAX and WLAN frequency band, respectively. A single SL is located at the bottom of the substrate that resonates at satellite communication X-band. Attenuation more than 20 dB is observed at all notched frequencies. An angular stability from 0° to 40° is obtained. Compact size, simple structure, low cost material, single layer, easy fabrication, and wide coverage are some of the feathers of this proposed FSS. The dimension of proposed unit cell of FSS is $10 \times 10 \text{ mm}^2$.

1. INTRODUCTION

In 2002, Federal Communications Commission (FCC) liberated UWB spectrum (3.1–10.6 GHz) for unlimited commercial use [1]. Since then, many researchers have shown keen interest in the UWB frequency range to enable the use of this frequency band in various applications [2, 3]. Wireless communication is one such promising application. Some of the key features of UWB antennas are wide impedance bandwidth, low cost, and low power consumption. However, some applications such as those working at WiMAX (3.3–3.6 GHz), WLAN (5–6 GHz), and satellite communication X-band (7.2–8.4 GHz) create interference problems with UWB antennas [4]. Therefore, it is required to filter out these interfering frequencies. FSS, which is a periodic structure [5], acts as one such spatial filter for the incident wave. When a wave is incident over the FSS surface, the wave either reflects back (band-stop) or transmits (band-pass) the signal completely or partially, depending upon the design of its array. Metal or aperture is embedded over the dielectric substrate to work as band-stop or bandpass filter, respectively [6]. Other applications of FSS are antenna reflectors, radomes, electromagnetic shields, absorbers, polarizer, and in communication [7–13].

In literature, a wide variety of FSS structures have been proposed specifically for bandstop and bandpass filtering applications [14, 15]. For miniaturized structure and bandpass behavior, different spiral shaped elements are combined to make an FSS [16, 17]. To stop WLAN frequency band through FSS, a modified swastika-shaped unit cell with 35° rotation of the arms is designed [18]. For electromagnetic shielding, a combination of capacitive and inductive patches is used to create an FSS [19]. However, the aforementioned structures resonate at single frequency, have narrow bandwidth, and are complex for fabrication.

With the advancement in wireless communication technologies, multiband FSS is in demand. Fractal structures [20], perturbed elements [21], and incorporation of multiresonant elements [22, 23] are

Received 11 September 2019, Accepted 25 November 2019, Scheduled 17 December 2019

* Corresponding author: Naveen Jaglan (naveenjaglan1@gmail.com).

The authors are with the Department of Electronics & Communication Engineering, Jaypee University of Information Technology, Wakanaghat, Solan, Himachal Pradesh, India.

some general structures which result in multiresonant operations. For dual band-stop characteristic [24], a cross dipole and a ring is embedded at either side of the substrate, to provide electromagnetic shielding at X-band and Ka-band. For triple band notches, a shorted square loop FSS is used [25]. Two square loops and one circular loop are embedded together to resonate at 2.45 GHz, 3.5 GHz, and 5.5 GHz [26]. These structures face some issues. For example, a large FSS structure is obtained due to huge unit cell size, and angular stability is quite low which affects the frequency response.

With the goal to provide an adequate solution for most of the issues mentioned above, this article introduces a compact triple band rejection single layer FSS at UWB frequency for a stable frequency response. The article is thus organized in the following order. Design and analysis of the unit cell of FSS are detailed in Section 2. Section 3 discusses the simulated and measured results. A comparison of different FSS structures with the present structure is also conducted to shed light on the advantages of the proposed FSS structure. Finally, the manuscript is concluded in Section 4.

2. DESIGN AND ANALYSIS

Figure 1 shows the design topology of the proposed unit cell FSS. A single layer FR-4 of dielectric constant of 4.4, thickness of 1.6 mm, and loss tangent of 0.02 is used as a substrate for the proposed structure. The dimension of the unit cell is $10 \times 10 \text{ mm}^2$, which is 0.1 times of the maximum operating wavelength of this proposed prototype. The top layer consists of two SSRRs (SSRR₁ and SSRR₂) having gap bearing sides opposite to each other. D_1 and D_2 are the lengths of arms of the SSRRs, G_1 and G_2 are the gaps in between the SSRRs, and S_1 and S_2 are the widths of the SSRRs. On the bottom plane of the substrate, an SL is imprinted. D_3 is the arm length of SL, and S_3 is the width of this loop. P is the period of the FSS. The values of all the parameters are listed in Table 1. Figure 2 shows the fabricated prototype of the proposed FSS structure.

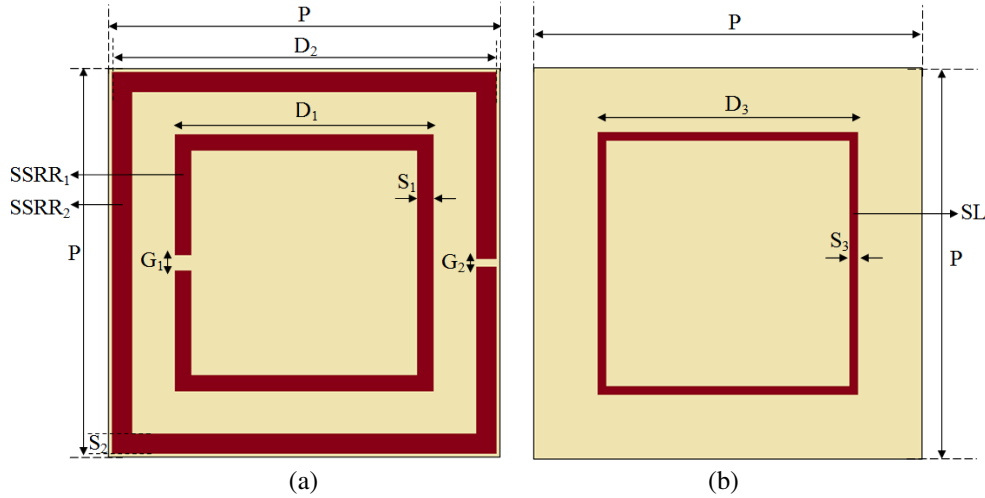


Figure 1. Configuration of the unit cell FSS. (a) Top view and (b) bottom view.

Table 1. Fabricated prototype of the proposed FSS.

Parameters	P	D_1	D_2	D_3	S_1	S_2	S_3	G_1	G_2
Value (mm)	10	6.6	9.8	6.7	0.4	0.5	0.2	0.4	0.2

For more details on the implementation of the present structure, three different steps in the designing are shown in Figure 3. In step 1 SSRR₁ is imprinted over an FR-4 substrate. SSRR₂ with a slit in opposite direction is then imprinted on the top plane of the FR-4 substrate. Finally, a square loop is embedded at the bottom plane of the FSS in step 3.

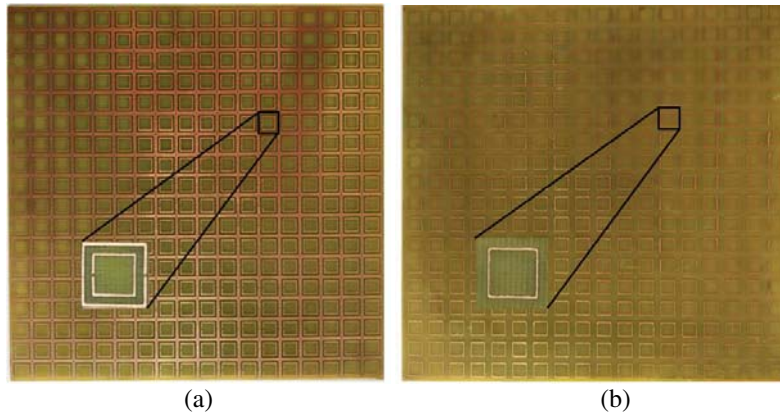


Figure 2. Fabricated prototype of the proposed FSS.

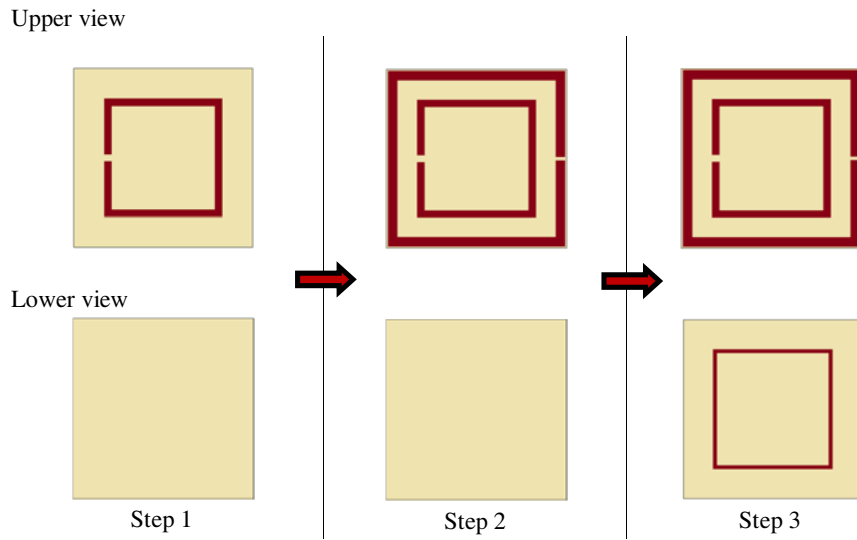


Figure 3. Formation of the proposed unit cell.

2.1. Design of the Proposed FSS

2.1.1. Design of SSRR

For smaller frequencies, it is slightly difficult to obtain a minimized design. Therefore, to achieve a compact design for the frequency bands such as WiMAX and WLAN, SSRRs have been used. To decrease the resonance frequency, slots are created in metallic loops. These gaps result in increased equivalent capacitance; therefore, resonance frequency shifts downwards. Here, two SSRRs are located at the top plane of the FSS substrate. Since the substrate is dielectric, its thickness is opted according to the relation $t < \lambda_0/20$. This is done to eliminate the effect of evanescent waves. Evanescent fields become more powerful in thicker materials and thereafter affect the performance [3]. Here t is the width of the FR-4 substrate, and λ_0 is the free space wavelength. For both SSRRs, the self inductance [27, 28] due to the metallic rings is given by:

$$L_1 = \frac{\mu_0 D_1}{\sqrt{\pi}} \left[\log \left(\frac{32 D_1}{S_1 \sqrt{\pi}} \right) - 2 \right] \tag{1}$$

$$L_2 = \frac{\mu_0 D_2}{\sqrt{\pi}} \left[\log \left(\frac{32 D_2}{S_2 \sqrt{\pi}} \right) - 2 \right] \tag{2}$$

where L_1 and L_2 are the inductance of the individual loop; D_1 and D_2 are the arm lengths; S_1 and S_2 are the arm width of individual rings. μ is the permeability in free space which is given by $4\pi \times 10^{-7} \text{ N/A}^{-2}$.

The two SSRRs are at a very close proximity of each other; therefore, capacitance in the top layer of the FSS is due to the self capacitance of the gaps and mutual capacitance in between the two rings. The self capacitance is given by:

$$C_{g1} = \varepsilon \frac{S_1 t}{G_1} \quad \text{and} \quad C_{g2} = \varepsilon \frac{S_2 t}{G_2} \quad (3)$$

C_{01} and C_{02} are the distributive capacitance in between the two SSRRs and are also a function of gap G . The mutual capacitance is given by:

$$C_{01} = \varepsilon \frac{S_1(2D_1 + 2D_2 - G_1)}{2t} \quad \text{and} \quad C_{02} = \varepsilon \frac{S_2(2D_1 + 2D_2 - G_2)}{2t} \quad (4)$$

C_1 and C_2 are the total of self inductance and mutual inductance in SSRRs and are given by

$$C_1 = C_{01} + C_{g1} \quad (5)$$

$$C_2 = C_{02} + C_{g2} \quad (6)$$

The resonance frequencies of SSRR₁ and SSRR₂ are calculated as:

$$f_{SSRR_1} = \frac{1}{2\pi\sqrt{L_1 C_1}} \quad (7)$$

$$f_{SSRR_2} = \frac{1}{2\pi\sqrt{L_2 C_2}} \quad (8)$$

2.1.2. Design of SL

SL is a conventional design which offers single band rejection frequency response depending upon the dimension of the structure and reflects back the incident wave at the resonant frequency [5]. To achieve the desired resonance, the perimeter of the SL is made equal to its wavelength. In the proposed bandstop FSS design, an SL is imprinted at bottom layer. Equations (9) and (10) show the relationship of L_3 and C_3 with P , S , and g [29].

$$\frac{w_r L_3}{Z_o} = D_3 \frac{\cos \theta}{\lambda} \left[\ln \left(\cos ec \left(\frac{\pi S_3}{2P} \right) \right) + G(P, S_3, \lambda, \theta) \right] \quad (9)$$

$$\frac{w_r C_3}{Y_o} = 4D_3 \frac{\sec \theta}{\lambda} \left[\ln \left(\cos ec \left(\frac{\pi g}{2P} \right) \right) + G(P, g, \lambda, \theta) \right] \varepsilon_{eff} \quad (10)$$

here ε_{eff} is the effective permittivity of the substrate material, and L_3 and C_3 are the equivalent inductance and capacitance of the SL. Z and Y are the characteristic impedance and admittance; P is the periodicity; g is the gap between two adjacent SLs; θ is the angle of incidence; and G is the correction factor given by [29]

$$G = \frac{(1 - \beta^2) \left[\left(1 - \frac{\beta^2}{4} \right) (A_+ + A_-) + 4\beta^2 A_+ A_- \right]}{\left(1 - \frac{\beta^2}{4} \right) + \beta^2 \left(1 + \frac{\beta^2}{2} - \frac{\beta^4}{8} \right) (A_+ + A_-) + 2\beta^6 A_+ A_-} \quad (11)$$

where

$$A_{\pm} = \frac{1}{\left[1 \pm \frac{2P \sin \theta}{\lambda} - \left(\frac{P \cos \theta}{\lambda} \right)^2 \right]^{1/2}} - 1 \quad (12)$$

$$\beta = \frac{\sin \pi S_3}{2P} \quad (13)$$

Multiplying Equations (9) and (10)

$$w_r^2 L_3 C_3 = 4 \left(\frac{D_3}{\lambda} \right)^2 \ln \left[\cos ec \left(\frac{\pi S_3}{2P} \right) + G(P, S_3, \lambda, \theta) \right] \cdot \ln \left[\cos ec \left(\frac{\pi g}{2P} \right) + G(P, g, \lambda, \theta) \right] \varepsilon_{eff} \quad (14)$$

For the resonant condition, left-hand side of Equation (9) should be made equivalent to 1.

$$w_r^2 L_3 C_3 = 1 \quad \text{or} \quad f_{SL} = \frac{1}{2\pi\sqrt{L_3 C_3}} \quad (15)$$

Therefore, the resonant wavelength is evaluated through Equation (16)

$$1 = 4 \left(\frac{D_3}{\lambda} \right)^2 \ln \left[\cos ec \left(\frac{\pi S_3}{2P} \right) + G(P, S_3, \lambda, \theta) \right] \cdot \ln \left[\cos ec \left(\frac{\pi g}{2P} \right) + G(p, g, \lambda, \theta) \right] \varepsilon_{eff} \quad (16)$$

To avoid the grating lobes, P is selected according to the following equation:

$$P(1 + \sin \theta) < \lambda \quad (17)$$

As the incident plane wave strikes the FSS, electrons in the metal surface start oscillating, and the surface currents get induced in the metallic loops. At the resonant frequencies f_{SSRR1} , f_{SSRR2} , and f_{SL} which are calculated from Equations (7), (8), and (15), these induced currents reradiate back the electromagnetic wave. Hence three notches are obtained at WiMAX, WLAN, and satellite communication X-band. Figure 4 shows the equivalent circuit of the proposed FSS design.

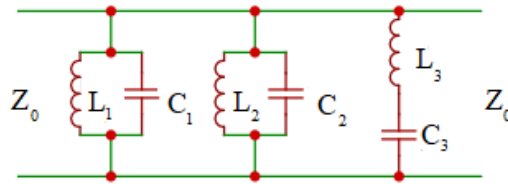


Figure 4. Equivalent circuit model for the proposed FSS [29, 30].

3. RESULTS AND DISCUSSIONS

3.1. Proposed Unit Cell Response (Step by Step Orientation of the FSS Unit Cell)

This proposed structure is simulated using Ansoft HFSS v.13 software, and S_{21} parameter is investigated for this design. It is observed that when step 1 is simulated, an individual resonance dip is obtained at

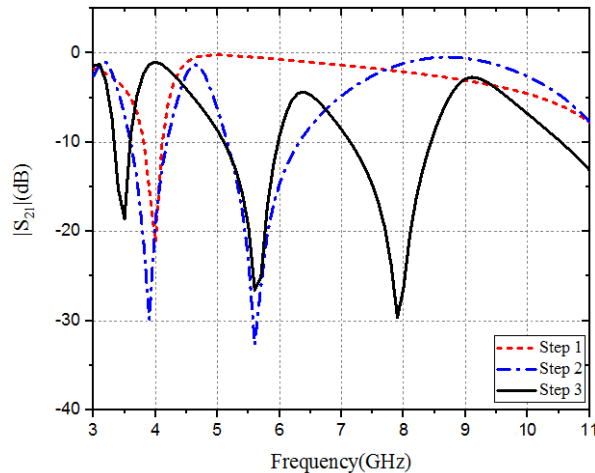


Figure 5. Step by step design of the proposed structure.

4 GHz due to the attachment of individual $SSRR_1$. In step 2, two resonance peaks appear at 3.9 GHz and 5.6 GHz, due to the presence of two different SSRRs. In step 3, triple notches are obtained at 3.4, 5.6, and 7.9 GHz, as shown in Figure 5. The resonant frequencies shift slightly due to the presence of mutual coupling in between the loops. After optimization of this structure, this FSS filter rejects three frequency bands, i.e., WiMAX (3.3–3.6 GHz), WLAN (5–6 GHz), and satellite communication X-band (7.2–8.4 GHz).

The surface current distribution reveals that $SSRR_1$ is responsible for resonating at 3.4 GHz, and $SSRR_2$ is responsible for resonating at 5.6 GHz, whereas SL makes the proposed structure resonate at 7.9 GHz, covering the entire range of UWB from 3.1 to 10.6 GHz as shown in Figure 6.

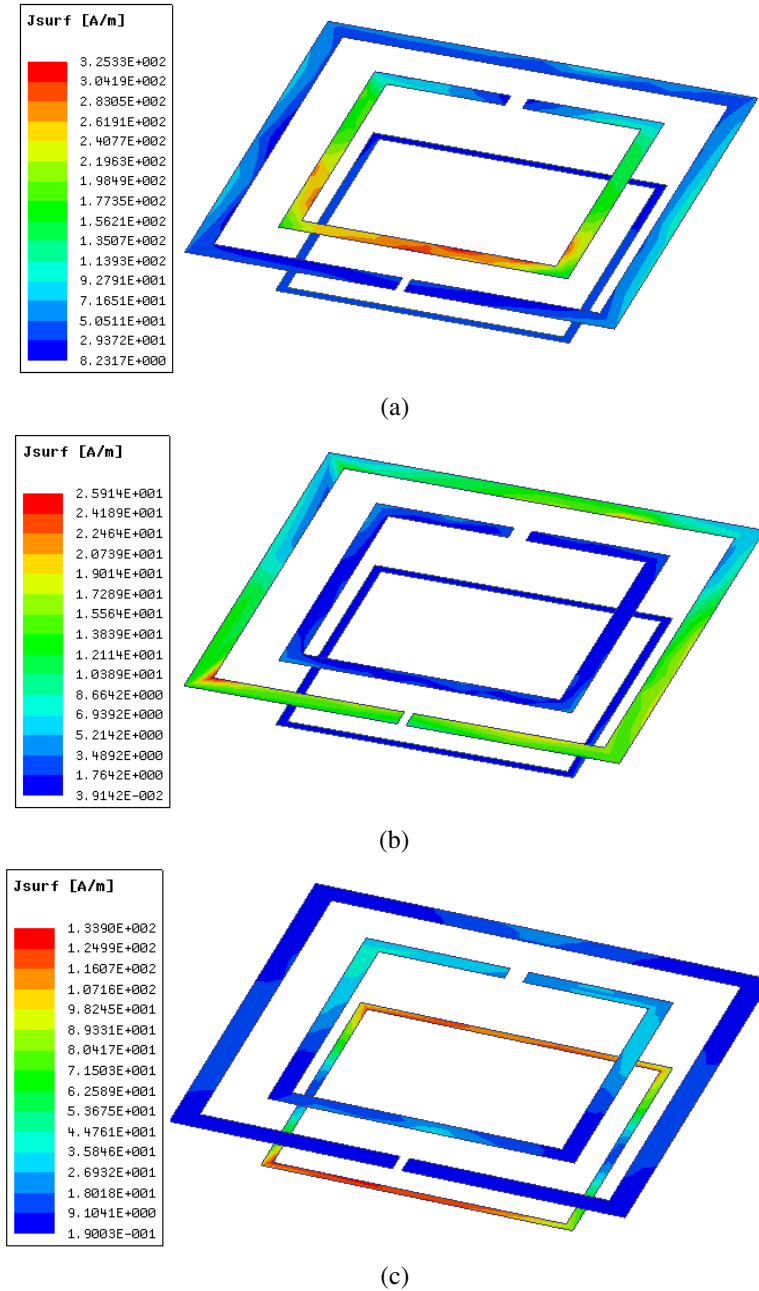


Figure 6. Surface current distribution of the proposed FSS unit cell at (a) 3.4 GHz, (b) 5.6 GHz and (c) 7.9 GHz.

3.2. Variation of the Length of the Loops

In Figures 7 and 8, the gaps G_1 and G_2 are varied while keeping D_1 and D_2 constant, respectively. It is observed that as the gap increases the capacitance of the structure decreases, and by Equations (7) and (8), it is evident that as the capacitance decreases the resonance frequencies shift to the upper range of frequency. By varying G_1 and G_2 , it is observed that the resonance frequencies only shift in WiMAX and WLAN bands, respectively. Therefore, every loop is responsible for its own resonance; however due to the mutual coupling between the loops, there is a slight shift in other bands as well, but is negligible. In Figure 9, D_3 is varied while keeping other parameters constant. By increasing the electrical length of the SL, the inductance of loop increases, and by Equation (15) again it is clear that the resonance frequency shifts to the lower values.

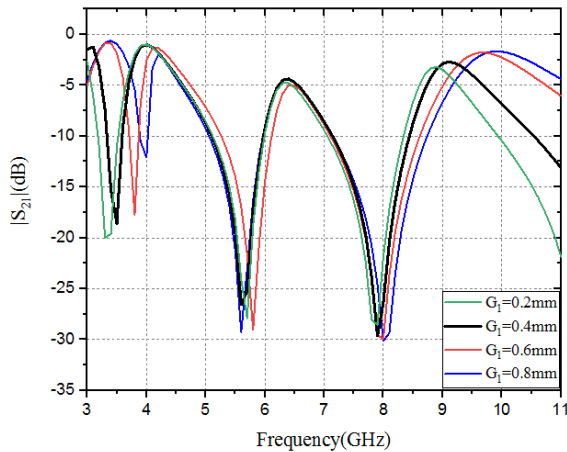


Figure 7. Variation of the gap G_1 while other parameters are constant.

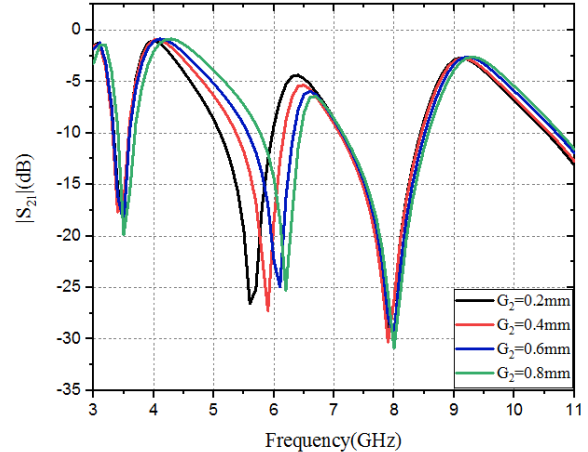


Figure 8. Variation of the gap G_2 while other parameters are constant.

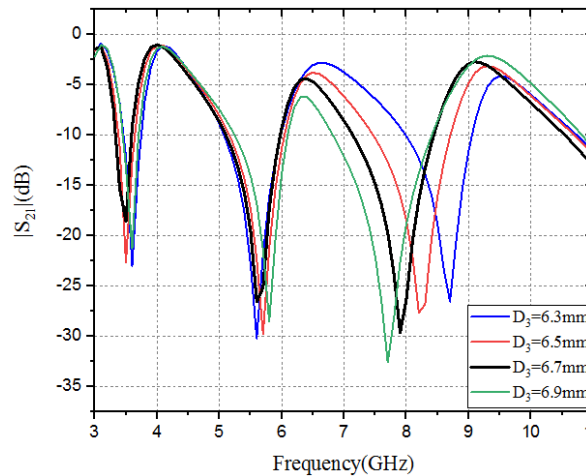


Figure 9. Variation of D_3 while S_3 is fixed.

3.3. Angular Stability

For specific applications, FSS needs to be installed at a particular position. However, the structure should provide same frequency response when being illuminated with different incident angles. Therefore, a stable frequency response is a requirement from FSS structure under the varying

environmental conditions. As a result, Figure 10 spotlights the variation of incident angles on the proposed FSS structure. Here the angular variation of 10° is depicted starting from 0° to 60° . It is observed that this structure when being illuminated with incident wave provides a similar frequency response up till 40° . Above this angle, there is a slight variation of the resonant frequencies which is clearly observed at 6 GHz. As the frequency response remains constant and stable and is not influenced by the environment factor, this structure is stable till 40° of angle of incidence.

3.4. Fabricated Results and Verification

For the validation of the simulated results, the proposed FSS is fabricated. The simulated and fabricated results are together shown in Figure 11. For the testing of the proposed prototype, two horn antennas are used as transmitter and receiver, and the results are then displayed in Agilent vector network (VNA). The transmitting horn antenna illuminates the signals on FSS. The signal with frequencies on the passband, passes the FSS, and reaches the receiving horn antenna whereas the others are obstructed by FSS. The curves of the simulated and measured S_{21} parameters are depicted in Figure 11. The results are obtained at an incident angle of 0° . It is observed that these two curves are at good agreement in terms of results.

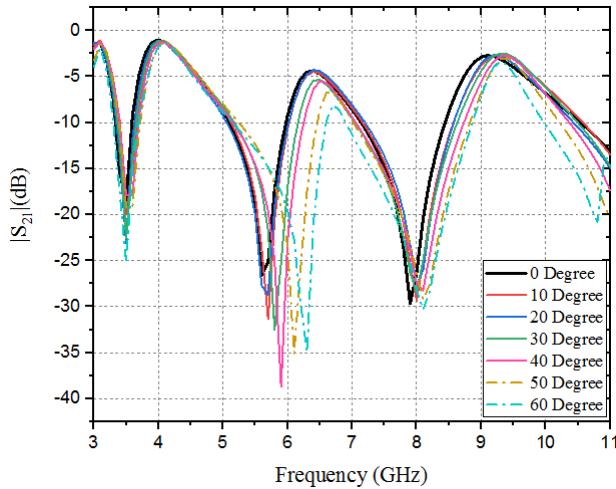


Figure 10. Variation of the incident angles on the FSS.

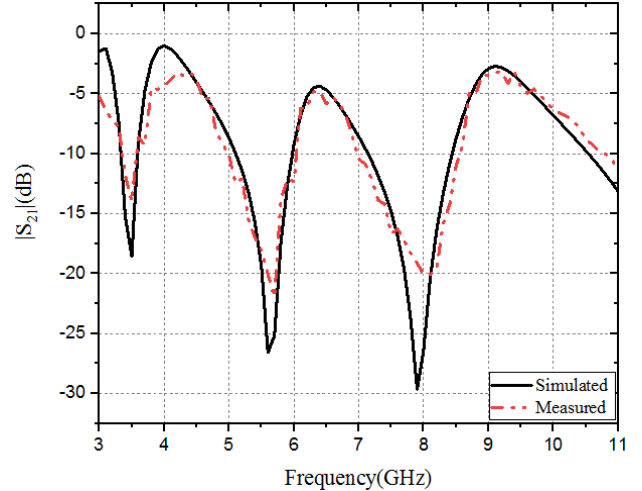


Figure 11. Simulated and measured values of the proposed design.

3.5. Comparison of Different FSSs

A comparative study of different FSS unit cell structures is performed in Table 2. Comparison is done for [18, 31–34] on the basis of size of the unit cell, resonant frequency, number of operating bands, attenuation, angular stability, and bandwidth. It is clearly observed that the FSS structures in [18, 31] resonate at an individual frequency, whereas those in [32, 33] resonate at two different frequencies. Compared to the resonant notches of the FSS structures shown in [18, 31–33], the proposed FSS design provides more resonant notches over the entire UWB range. The unit cell of [32, 33] occupies the size larger than the proposed one; consequently, the proposed FSS provides wider bandwidth with better angular stability. The design suggested by the authors in [34] shows three different band rejection notches at WiMAX, WLAN, and X-band over the entire UWB. Although the structure is quite compact, the wastage of the transmission band is huge. The frequency range of the WiMAX, WLAN, and X-band is 3.3 to 3.6 GHz, 5 to 6 GHz, and 8 to 12 GHz, respectively, and the range of X-band satellite communication band is 7.2 to 8.4 GHz. The proposed FSS in this paper improves the transmission bandwidth by minimizing the wastage of frequencies at band notches. Further, the angular stability in [32] is also quite low. Table 2 also depicts that the proposed design has a decent angular stability. Therefore, the proposed prototype is suitable for filtering application at UWB frequency range.

Table 2. Comparative study of various FSS.

Ref.	Unit cell dimension (mm ³)	Resonant frequency (GHz)	No. of operating bands	Operating band	Angular Stability	Attenuation (dB)	Rejection Bandwidth
[18]	7 × 7 × 1.6	5	1	WLAN	0°–60°	20	400 MHz
[31]	6.8 × 6.8 × 0.127	10	1	X-band	0°–60°	56	4 GHz
[32]	8.8 × 8.8 × 0.762	8.47, 10.45	2	Wideband X-band	0°–60°	47	7.5–9.4 GHz, 10.4–10.8 GHz
[33]	20 × 20 × 2	2.45, 5.5	2	Wi-Fi and WLAN	0°–45°	43	630 MHz, 1430 MHz
[34]	10 × 10 × 1.6	3.5, 5.2, 10.2	3	WLAN, WiMAX, X-band	0°–30°	60	0.5 GHz (3.1–3.7), 1.9 GHz (4.1–6), 4.1 GHz (8–12.1)
Proposed work	10 × 10 × 1.6	3.45, 5.5, 8	3	WiMAX, WLAN, Satellite comm. X-band	0°–40°	30	0.3 GHz (3.3–3.6), 1 GHz (5–6), 1.2 GHz (7.2–8.4)

4. CONCLUSION

Triple band rejection notches have been obtained by embedding two SSRRs at the top plane and single SL at the bottom plane of the substrate. The fabrication of this structure is performed over a low cost, commercially available FR-4 substrate of the dimension 10 × 10 × 1.6 mm³. The triple band rejection notches are observed at WiMAX band, WLAN, and X-band satellite communication band, ranging from 3.3–3.6 GHz, 5–6 GHz and 7.2–8.4 GHz, respectively. A stable frequency response up till 40° has been obtained. The results show good agreement between simulated and measured values, therefore, making it suitable for the communication applications.

ACKNOWLEDGMENT

Sincere thanks to Prof. Binod K. Kanaujia (Jawaharlal Nehru University) for permitting us to access the laboratory facilities.

REFERENCES

1. Federal Communications Commission, “Revision of part 15 of the commission’s rules regarding ultra-wideband transmission systems,” *Tech. Rep. ET-Docket 98-153*, FCC02-48, Federal Communications Commission (FCC), Washington, DC, USA, 2002.
2. Paul, G. S. and K. Mandal, “Polarization-insensitive and angularly stable compact ultra-wide stop-band frequency selective surface,” *IEEE Antennas and Wireless Propagation Letters*, Vol. 18, No. 9, 1917–1921, Sept. 2019
3. Wu, W., B. Yuan, and A. Wu, “A quad-element UWB MIMO antenna with band-notch and reduced mutual coupling based on EBG structures,” *Int. J. Antennas Propag.*, Vol. 2018, 1–10, 2018.
4. Jaglan, N., S. D. Gupta, B. K. Kanaujia, S. Srivastava and E. Thakur, “Triple Band Notched DG-CEBG Structure Based UWB MIMO/Diversity Antenna”, *Progress In Electromagnetics Research C*, Vol. 80, 21–37, 2018
5. Munk, B. A., *Frequency Selective Surfaces: Theory and Design*, Vol. 29, Wiley Online Library: Hoboken, NJ, USA, 2000.
6. Munk, B. A., *Finite Antenna Arrays and FSS*, New York, Wiley, 2003.

7. Pasian, M., S. Monni, A. Neto, M. Ettorre, and G. Gerini, "Frequency selective surfaces for extended bandwidth backing reflector functions," *IEEE Trans. Antennas Propag.*, Vol. 58, No. 1, 43–50, Jan. 2010.
8. Sivasamy, R., B. Moorthy, M. Kanagasabai, V. R. Samsingh, and M. G. N. Alsath, "A wideband frequency tunable fss for electromagnetic shielding applications," *IEEE Transactions on Electromagnetic Compatibility*, Vol. 60, No. 1, Feb. 2018.
9. Chen, H., X. Hou, and L. Deng, "Design of frequency-selective surfaces radome for a planar slotted waveguide antenna," *IEEE Antennas and Wireless Propagation Letters*, Vol. 8, 1231–1233, 2009.
10. Duan, Z., G. Abomakhleb, and G. Lu, "Perforated medium applied in frequency selective surfaces and curved antenna radome," *Applied Sciences*, Vol. 9, No. 6, 1–12, 2019.
11. Zhang, K., W. Jiang, J. Ren, and S.-X. Gong, "Design of frequency selective absorber based on parallel LC resonators," *Progress In Electromagnetics Research M*, Vol. 65, 91–100, 2018.
12. Das, G., N. K. Sahu, A. Sharma, R. K. Gangwar, and M. S. Sharawi, "FSS based spatially decoupled back to back four port MIMO DRA with multi-directional pattern diversity," *IEEE Antennas and Wireless Propagation Letters*, Vol. 18, No. 8, 1552–1556, 2019.
13. Mondal, K., D. C. Sarkar, and P. P. Sarkar, " 5×5 matrix patch type frequency selective surface based miniaturized enhanced gain broadband microstrip antenna for WLAN/WiMAX/ISM band applications," *Progress In Electromagnetics Research C*, Vol. 89, 207–219, 2019.
14. Jiang, W., T. Hong, S.-X. Gong, and C.-K. Li, "Miniaturized frequency selective surface with a bionical structure," *Microw. Opt. Technol. Lett.*, Vol. 55, No. 2, 335–337, Feb. 2013.
15. Kiani, G. I., K. P. Esselle, K. L. Ford, A. R. Weily, and C. Panagamuwa, "Angle and polarization independent bandstop frequency selective surface for indoor wireless systems," *Microw. Opt. Technol. Lett.*, Vol. 50, No. 9, 2315–2317, Sep. 2008.
16. Chiu, C.-N. and K.-P. Chang, "A novel miniaturized-element frequency selective surface having a stable resonance," *IEEE Antennas and Wireless Propagation Letters*, Vol. 8, 1175–1177, 2009.
17. Yang, G., T. Zhang, W. Li, and Q. Wu, "A novel stable miniaturized frequency selective surface," *IEEE Antennas Wireless Propag. Lett.*, Vol. 9, 1018–1021, 2010.
18. Natarajan, R., M. Kanagasabai, S. Baisakhiya, R. Sivasamy, S. Palaniswamy, and J. K. Pakkathillam, "A compact frequency selective surface with stable response for WLAN applications," *IEEE Antennas and Wireless Propagation Letters*, Vol. 12, 718–720, 2013.
19. Li, W., T. Zhang, G. Yang, and Q. Wu, "A novel frequency selective surface with improved miniaturization performance," *J. Electromagn. Anal. Appl.*, Vol. 4, 108–111, 2012.
20. Gianvittorio, J. P., J. Romeu, S. Blanch, and Y. Rahmat-Samii, "Selfsimilar prefractal frequency selective surfaces for multiband and dualpolarized applications," *IEEE Trans. Antennas Propag.*, Vol. 51, No. 11, 3088–3096, Nov. 2003.
21. Hill, R. A. and B. A. Munk, "The effect of perturbing a frequencyselective surface and its relation to the design of a dual-band surface," *IEEE Trans. Antennas Propag.*, Vol. 44, No. 3, 368–374, Mar. 1996.
22. Sanz-Izquierdo, B., E. A. Parker, and J. C. Batchelor, "Dual-band tunable screen using complementary split ring resonators," *IEEE Trans. Antennas Propag.*, Vol. 58, No. 11, 3761–3765, Nov. 2010.
23. Huang, J., T.-K. Wu, and S.-W. Lee, "Tri-band frequency selective surface with circular ring elements," *IEEE Trans. Antennas Propag.*, Vol. 42, No. 2, 166–175, Feb. 1994.
24. Syed, I. S., Y. Ranga, L. Matekovits, K. P. Esselle, and S. G. Hay, "A single-layer frequency-selective surface for ultrawideband electromagnetic shielding," *IEEE Transactions on Electromagnetic Compatibility*, Vol. 56, No. 6, 1404–1411, 2014.
25. Sivasamy, R., B. Moorthy, M. Kanagasabai, V. R. Samsingh, and M. G. N. Alsath, "A wideband frequency tunable FSS for electromagnetic shielding applications," *IEEE Transactions on Electromagnetic Compatibility*, Vol. 60, No. 1, Feb. 2018.
26. Garg, S. and S. Yadav, "A triple band-reject frequency selective surface for broadband applications," *Optical and Wireless Technologies*, 437–446, 2018.

27. Patel, S. K. and Y. Kosta, "Liquid metamaterial based microstrip antenna," *Microwave and Optical Technology Letters*, Vol. 60, No. 2, 2018.
28. Wang, J., S. Qu, J. Zhang, H. Ma, Y. Yang, C. Gu, and X. Wu, "A tunable left handed metamaterial based on modified broadside-coupled split-ring resonators," *Progress In Electromagnetics Research Letters*, Vol. 6, 35–45, 2009.
29. Langley, R. and E. Parker, "Equivalent circuit model for arrays of square loops," *Electron. Lett.*, Vol. 18, No. 7, 294, 1982.
30. Lin, X. Q. and T. J. Cui, "Controlling the bandwidth of split ring resonators," *IEEE Microwave and Wireless Components Letters*, Vol. 18, No. 4, 245–247, 2008.
31. Nauman, M., R. Saleem, and A. K. Rashid, "A miniaturized flexible frequency selective surface for X-band applications," *IEEE Trans. Electromagn. Compat.*, Vol. 58, No. 2, 419–428, 2016.
32. Ünalđı, S., S. Çimen, G. Çakır, and U. E. Ayten, "A novel dual-band ultrathin FSS with closely settled frequency response," *IEEE Antennas Wireless Propag. Lett.*, Vol. 16, 1381–1384, 2017.
33. Farooq, U., M. F. Shafique, and M. J. Mughal, "Polarization insensitive dual band frequency selective surface for RF shielding through glass windows," *IEEE Transactions on Electromagnetic Compatibility*, 1–8, Feb. 2019.
34. Bashiri, M., C. Ghobadi, J. Nourinia, and M. Majidzadeh, "WiMAX, WLAN, and X-band filtering mechanism: Simple-structured triple-band frequency selective surface," *IEEE Antennas and Wireless Propagation Letters*, Vol. 16, 3245–3248, 2017.